Electronic Supplementary Material (ESI) for Chemical Communications

SUPPORTING INFORMATION FOR:

Microwave synthesis of Au-Rh core-shell nanoparticles and implications of the shell thickness in hydrogenation catalysis

Stephany García,[a] Rachel Anderson,[a] Hugo Celio,[b] Naween Dahal,[a] Andrei Dolocan,[b] Jiping Zhou,[b] and Simon M. Humphrey*[a]

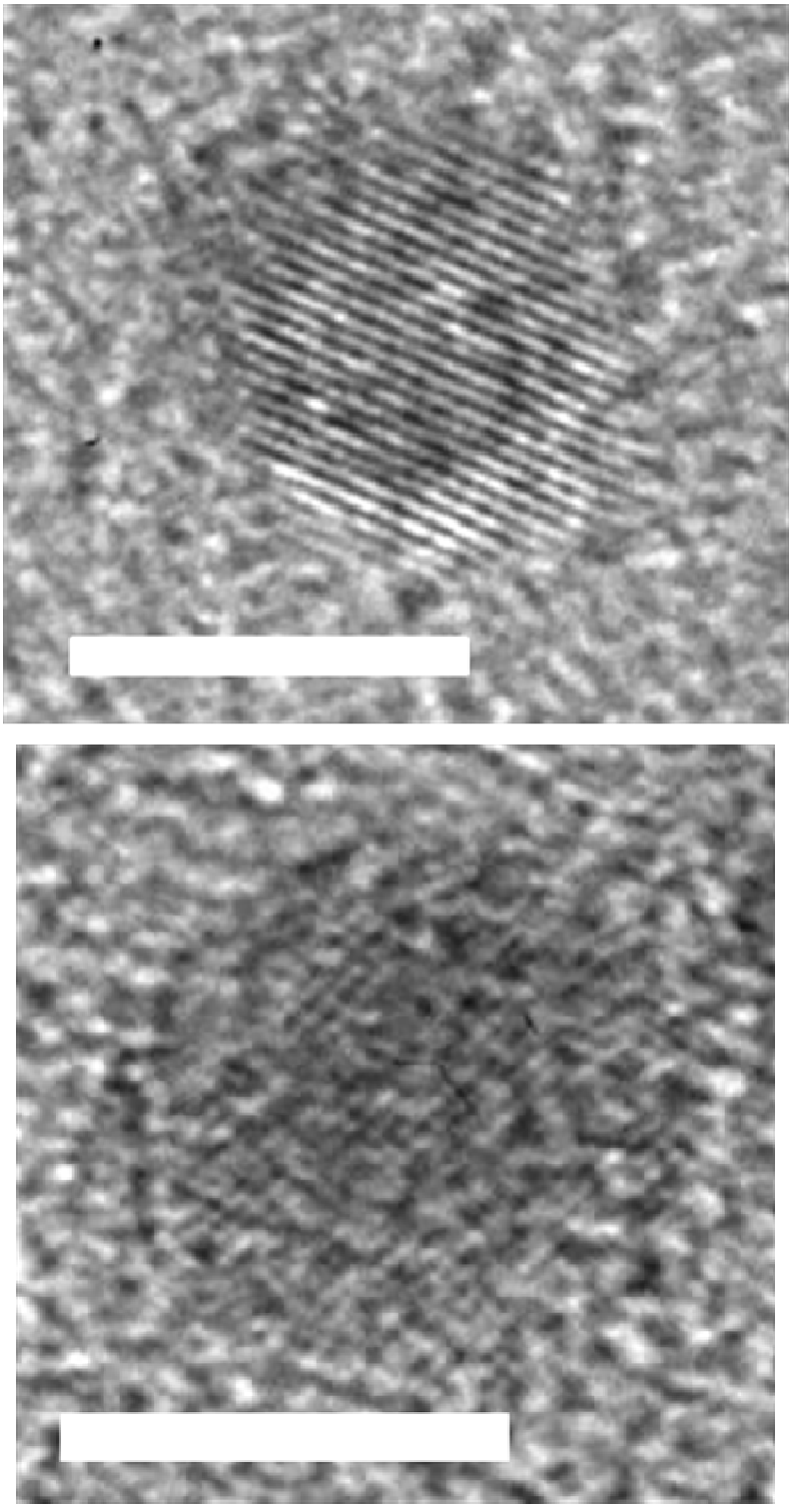

Fig S1. HRTEM images of thin Rh on Au NPs. The scale bars represent 5 nm.

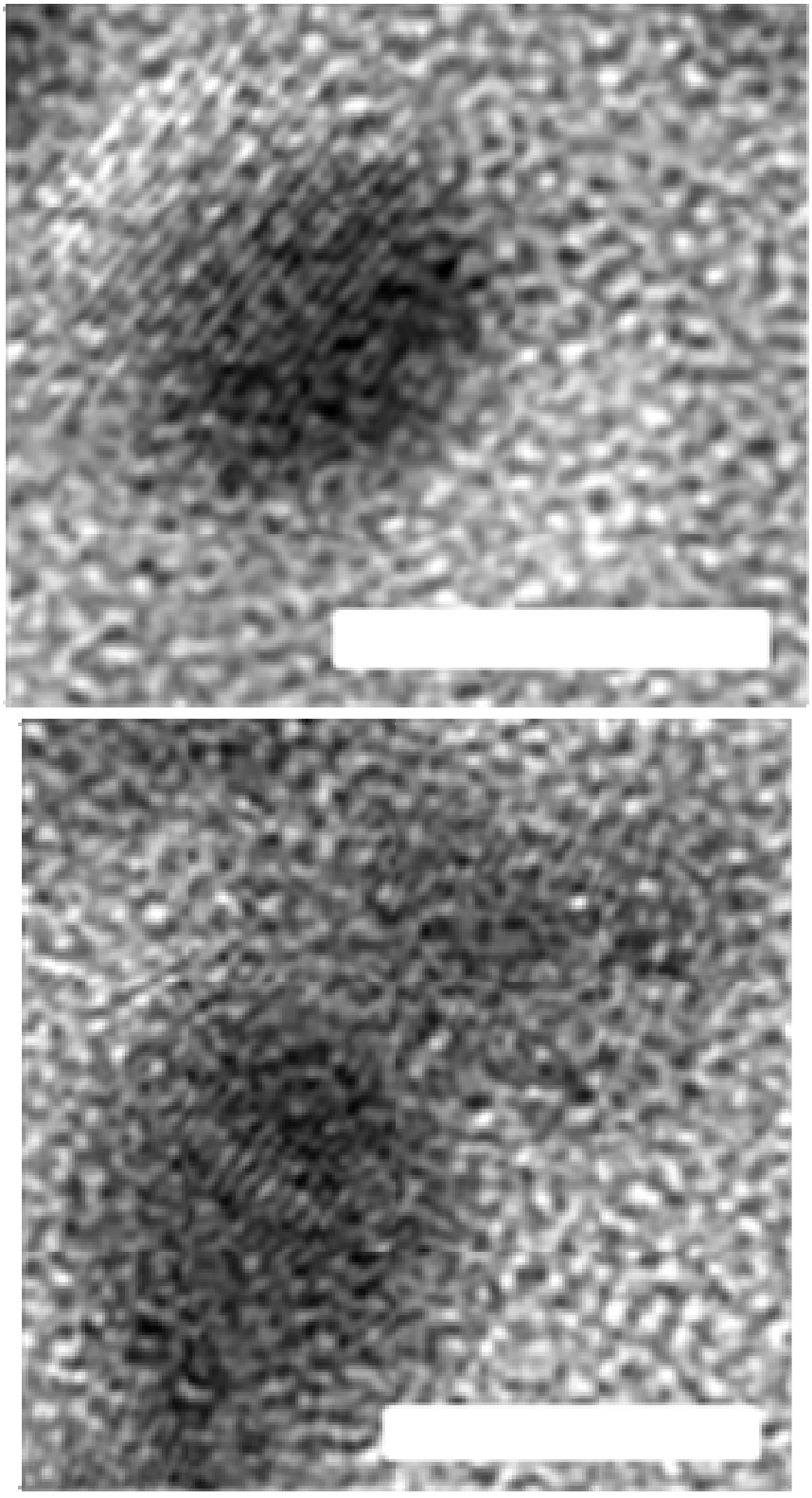

Fig S2. HRTEM images of Au-Rh core-shell NPs with a thick Rh layer. The scale bars represent 5 nm.

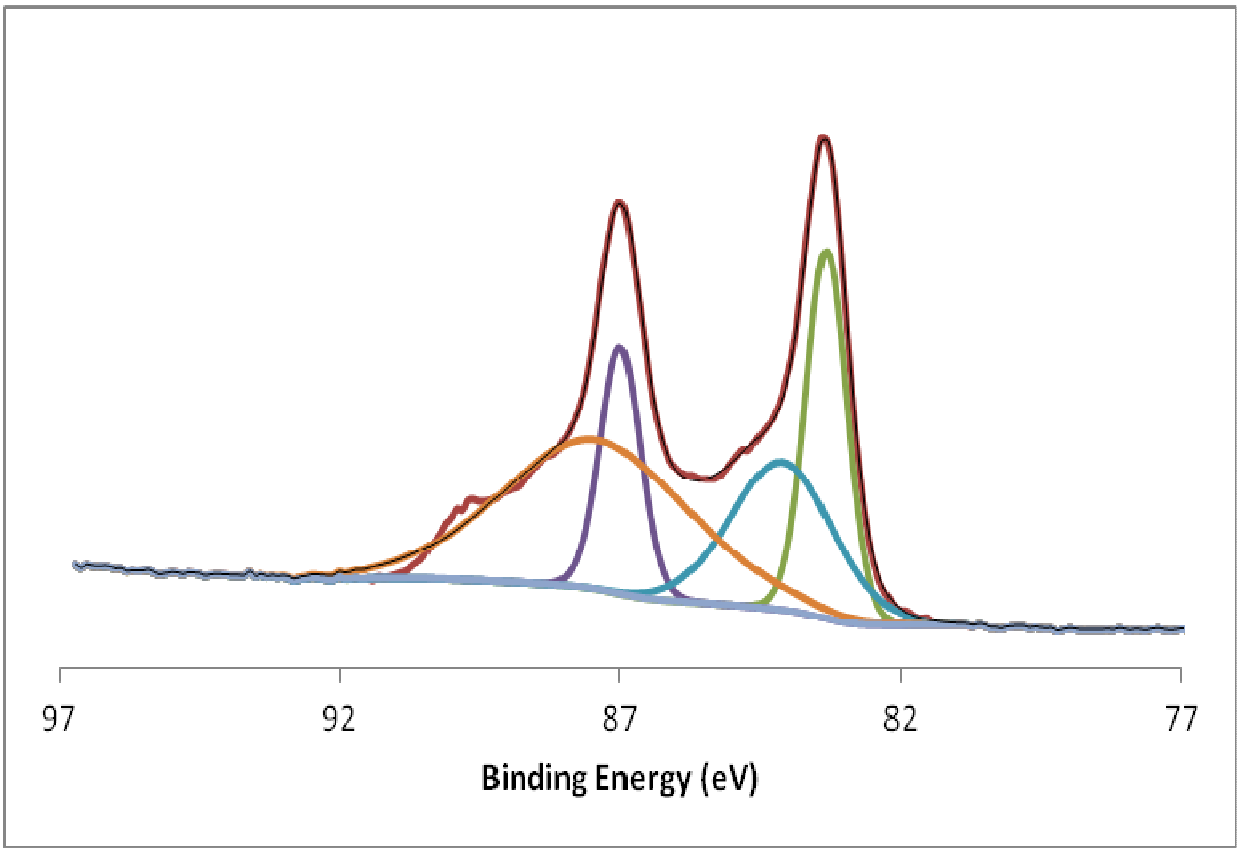

Figure S3. Fitted XPS data for PVP-capped MwH-AuNPs.

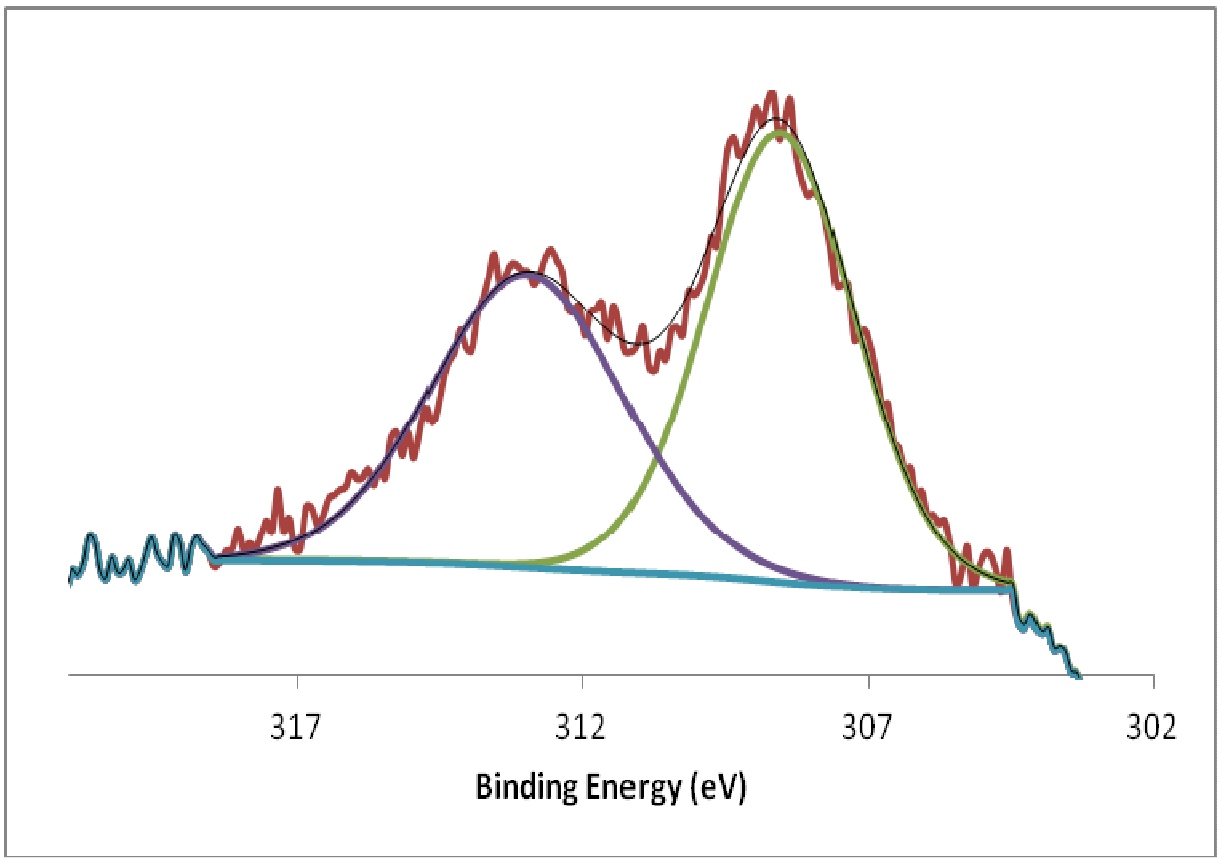

Figure S4. Fitted XPS data for pure PVP-capped RhNPs.

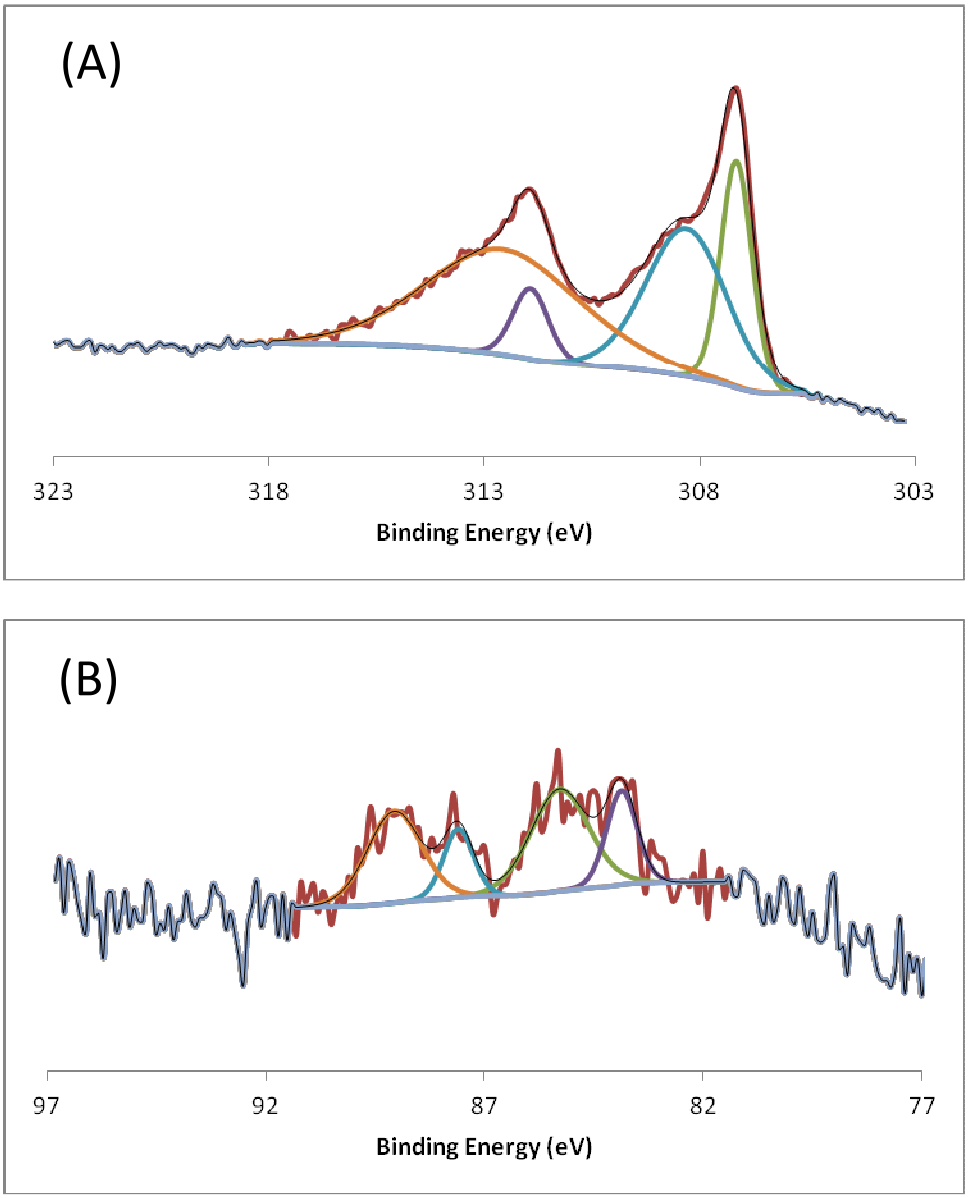

Figure S5. Fitted XPS data for Au-Rh core shell NPs with a thin Rh layer; (A) Rh 3d signals corresponding to metallic Rh (307.2 eV) and Rh(I) (308.5 eV); (B) Au 4f signals indicating the presence of both Au(0) (83.9 eV) and Au (I) (85.3 eV).

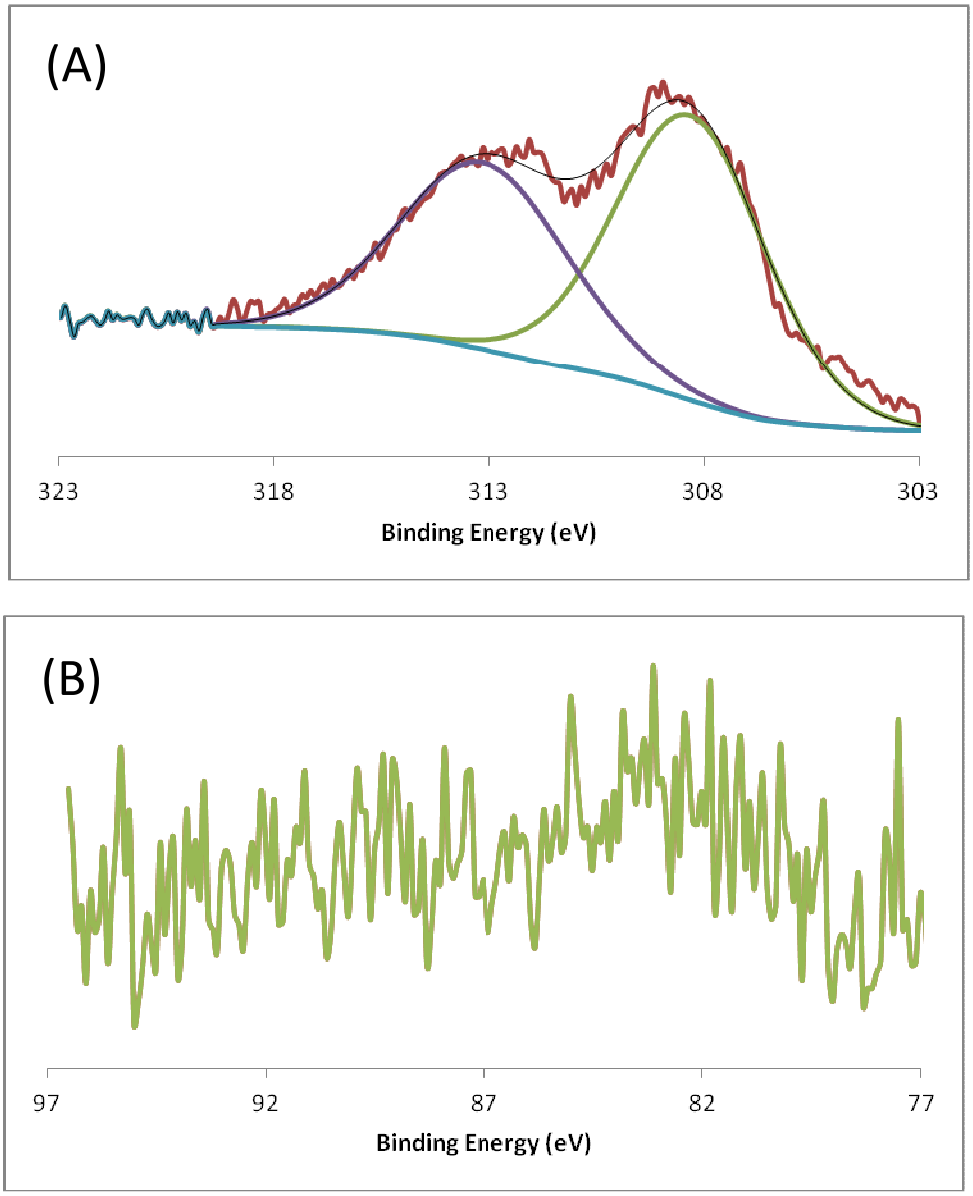

Figure S6. Fitted XPS data for Au-Rh core-shell NPs with a thick Rh layer; (A) Rh 3d signals assigned to Rh(I) (308.3 eV); (B) Absence of Au 4f signal.

Table S1. Rh(I):Rh(0) and Au(X):Rh(X) ratios, based on XPS values, for both thin-Rh and thick-Rh core-shell NPs prior to catalytic studies.

	Rh(I) : Rh(0)	**Au : Rh**
Thin-Rh NPs	1.7 : 1	1 : 46
Thick-Rh NPs	1 : 0	0 : 1

Table S2. Rh and Au binding energy values (eV) for MwH-Au seeds, MwH-RhNPs, thin- and thick-Rh acquired from XPS data.

	$3d_{5/2}$ (0)	**$3d_{3/2}$ (0)**	**$3d_{5/2}$ (I)**	**$3d_{3/2}$ (I)**	**$4f_{7/2}$ (0)**	**$4f_{5/2}$ (0)**	**$4f_{7/2}$ (I)**	**$4f_{5/2}$ (I)**
PVP-capped RhNPs	--	--	308.5	313.0	--	--	--	--
PVP-capped AuNPs	--	--	--	--	84.0	87.6	85.0	88.6
Thin Rh on Au	307.2	311.9	308.2	312.6	83.9	87.6	85.3	89.1
Thick Rh on Au	--	--	308.3	313.1	--	--	--	--

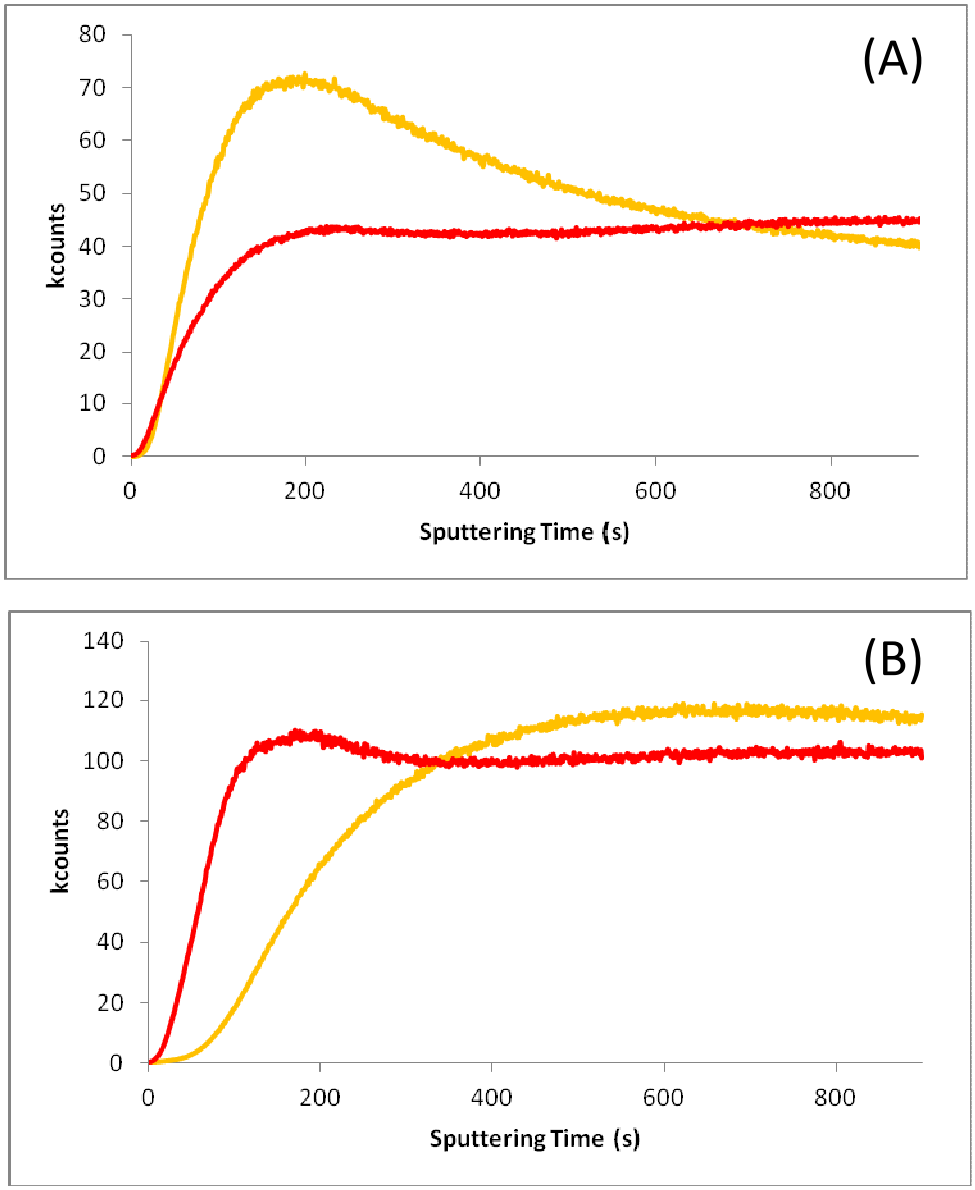

Figure S7. TOF SIMS: kcounts of Rh^- (red) and Au^- (yellow) ions plotted as a function of sputtering time; (A) Thin-Rh NPs; (B) Thick-Rh NPs.

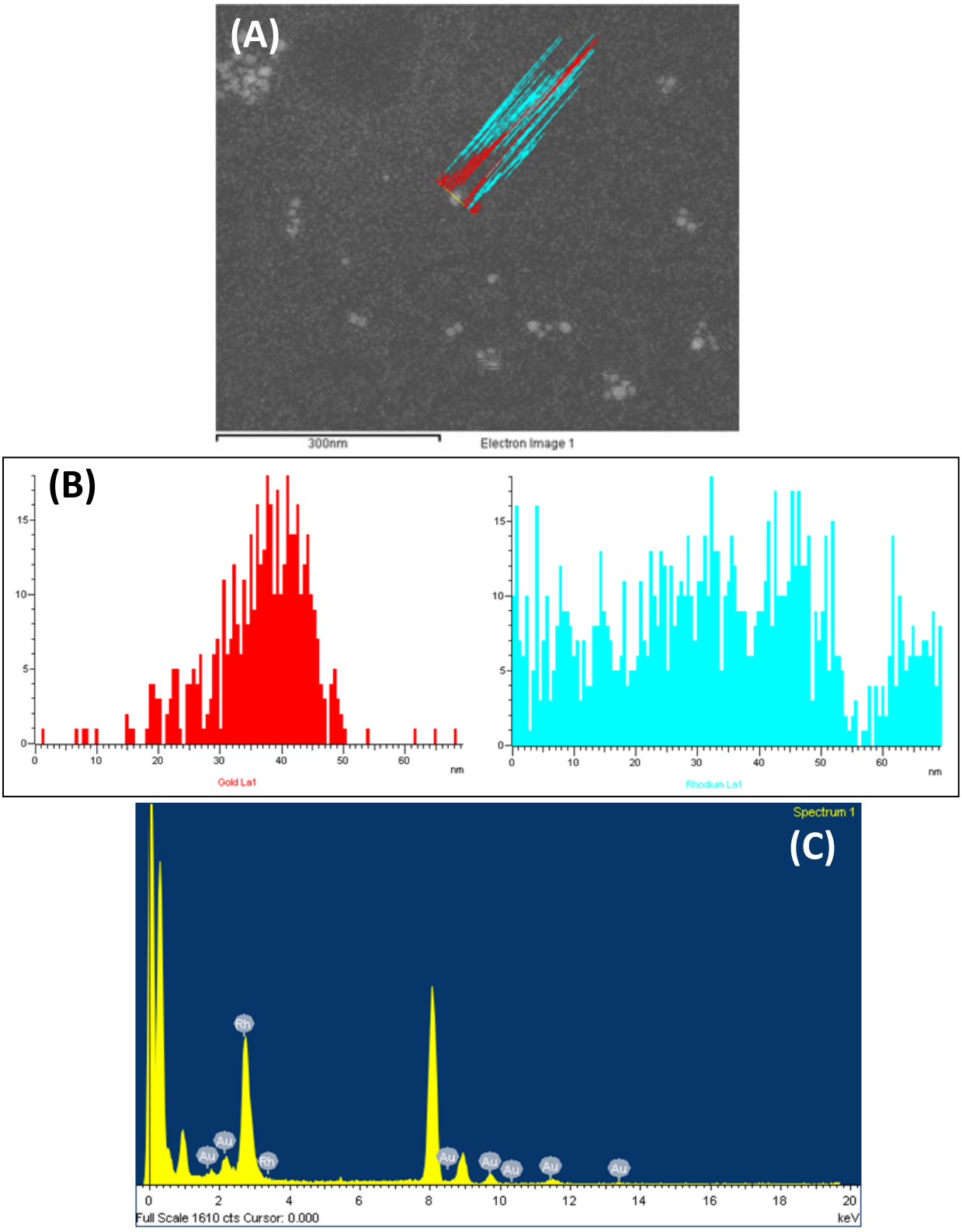

Fig S8. (A) TEM image and element profile of thin Rh; (B) Au and Rh elemental distribution and (C) spectrum of a single thin Rh on Au particle as given by EDS analysis. Any unlabeled peaks in the spectrum correspond to the C coated Cu grids used in TEM analysis.

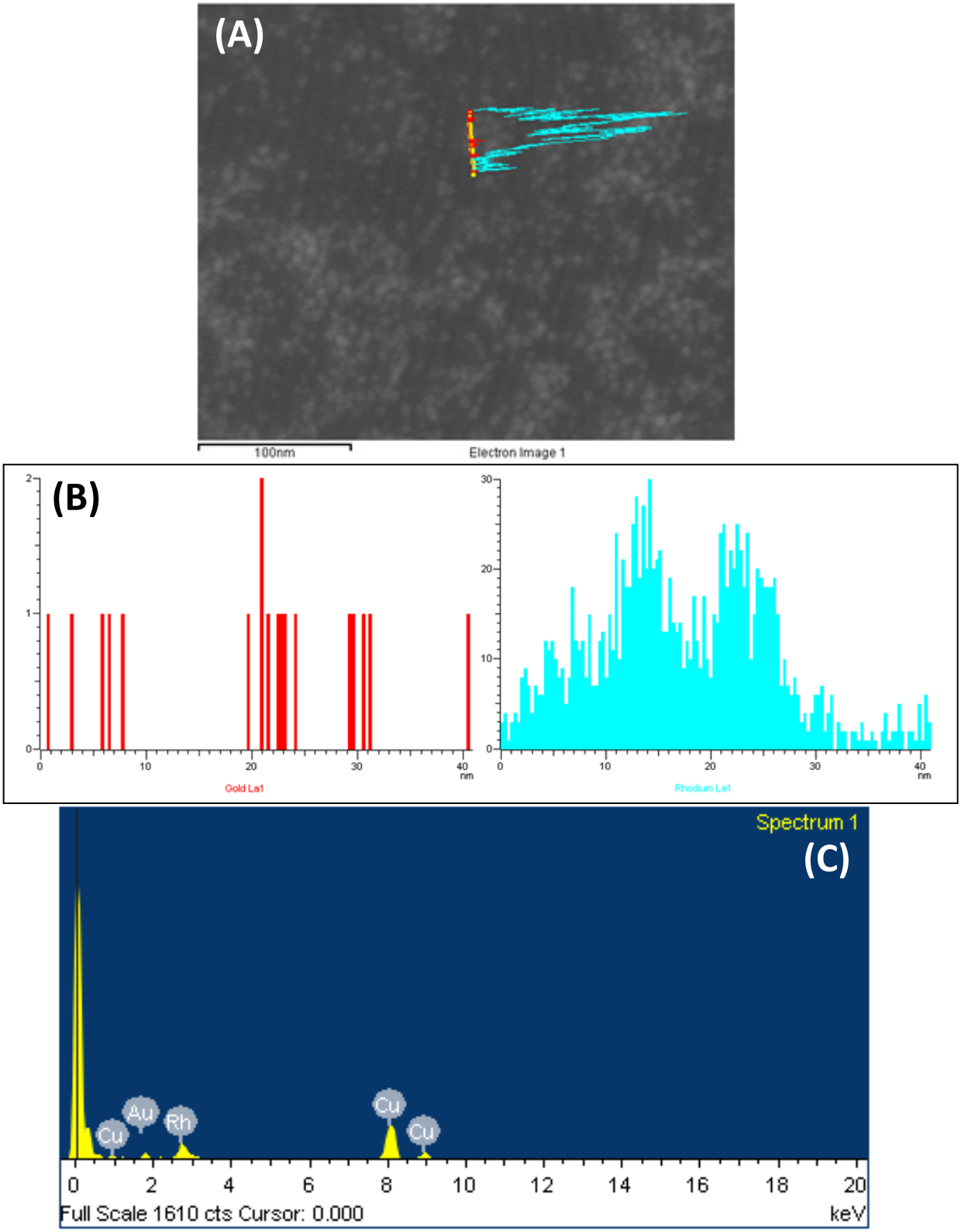

Fig S9. (A) TEM image and element profile of thick Rh; (B) Au and Rh elemental distribution and (C) spectrum of two thick-Rh particles in a row as given by EDS analysis. The Cu signals and other unlabeled peaks in the spectrum correspond to the C coated Cu grids used in TEM analysis.

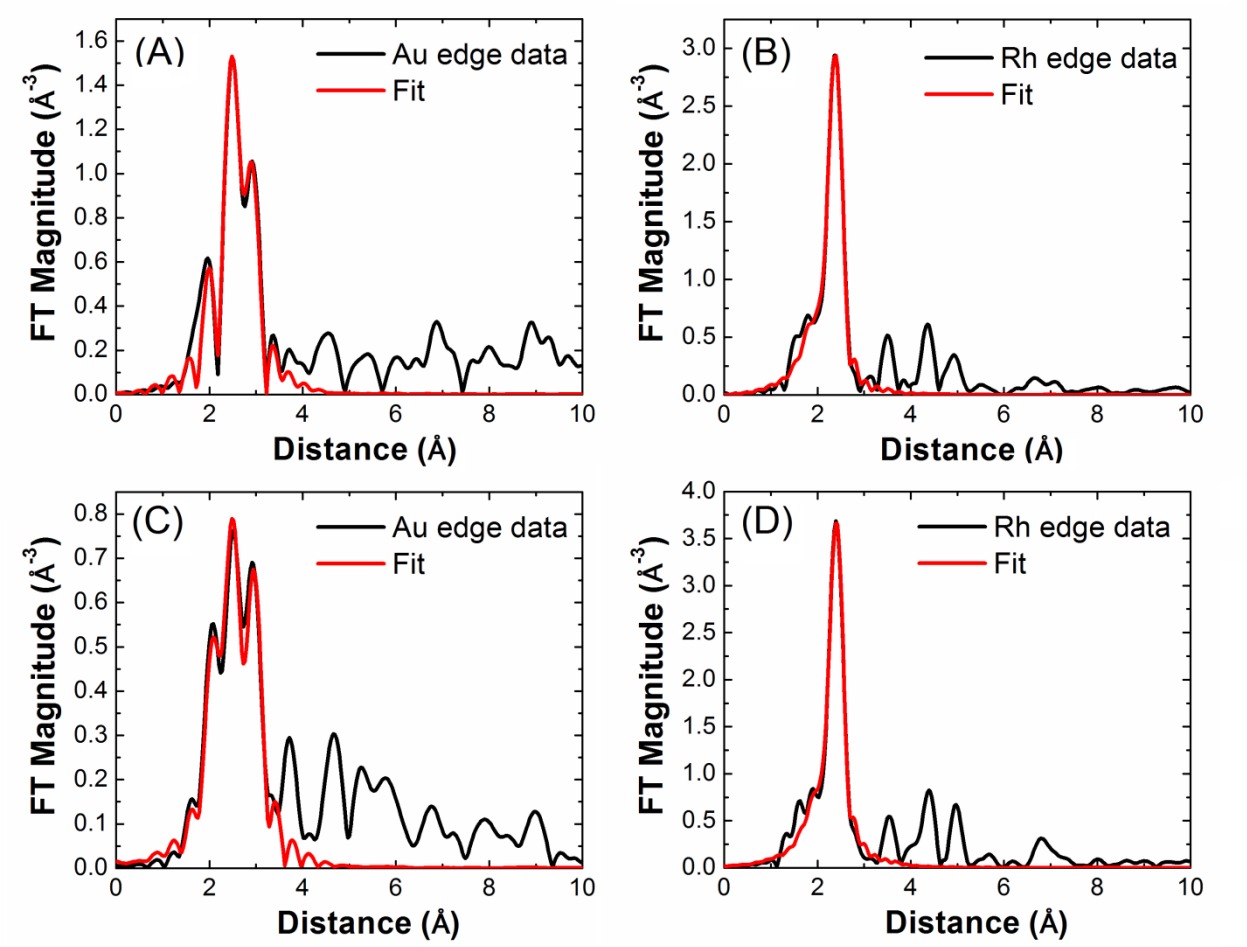

Figure S10. EXAFS analysis of (A and B) thin-Rh NPs and (C and D) thick-Rh NPs plotted in R-space. The black lines are the experimental data and the red lines are the calculated fits.

Table S3. Coordination numbers resulting from the EXAFS fitting analysis.

	CN_{Au-Au}	CN_{Au-Rh}	CN_{Rh-Rh}	CN_{Rh-Au}
Thin-Rh NPs	9.4 ± 5.0	1.0 ± 0.8	6.7 ± 0.8	0.7 ± 0.6
Thick-Rh NPs	11.0 ± 2.9	0.4 ± 0.4	7.9 ± 0.9	0.6 ± 0.8

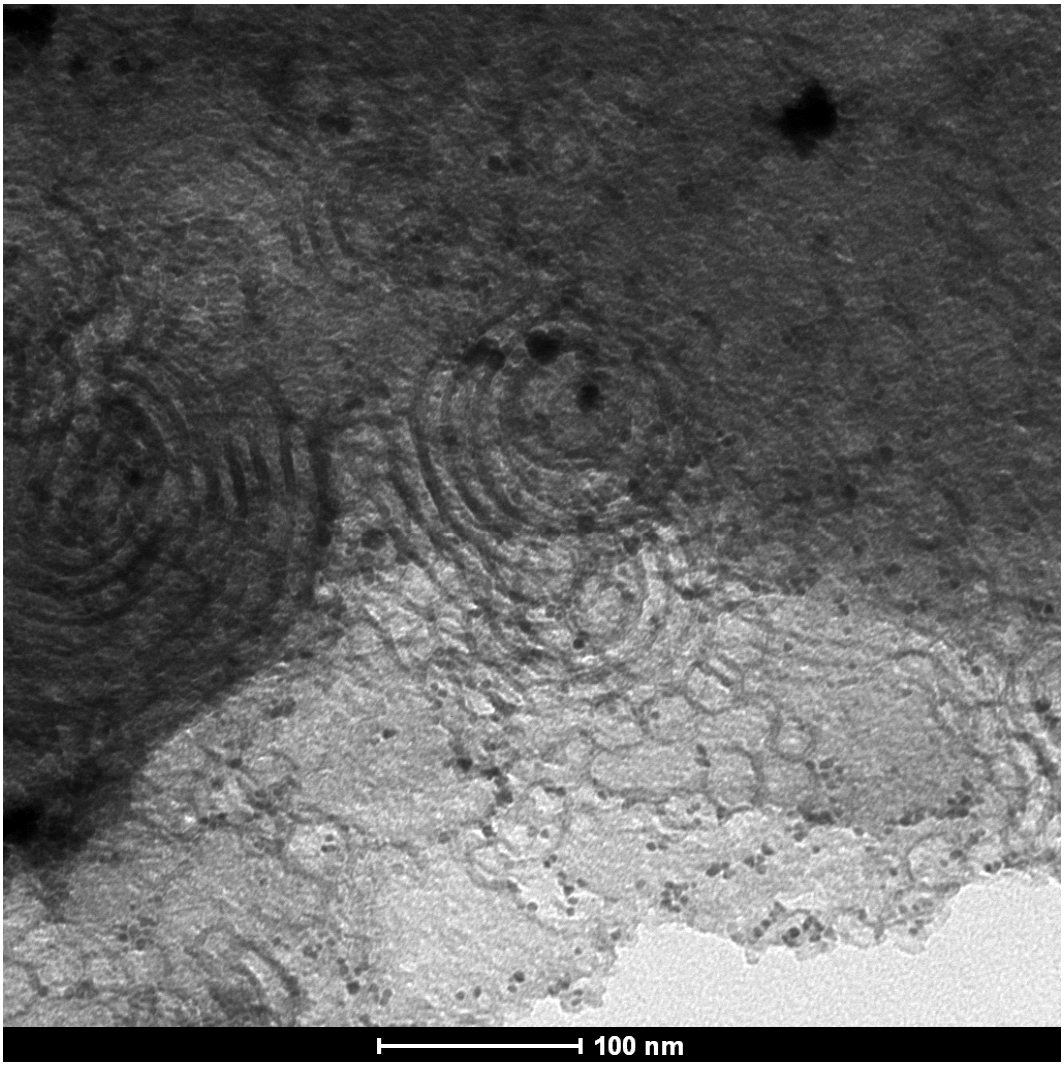

Figure S11. TEM image of Au-Rh core-shell NPs with a thin Rh layer supported on amorphous silica.

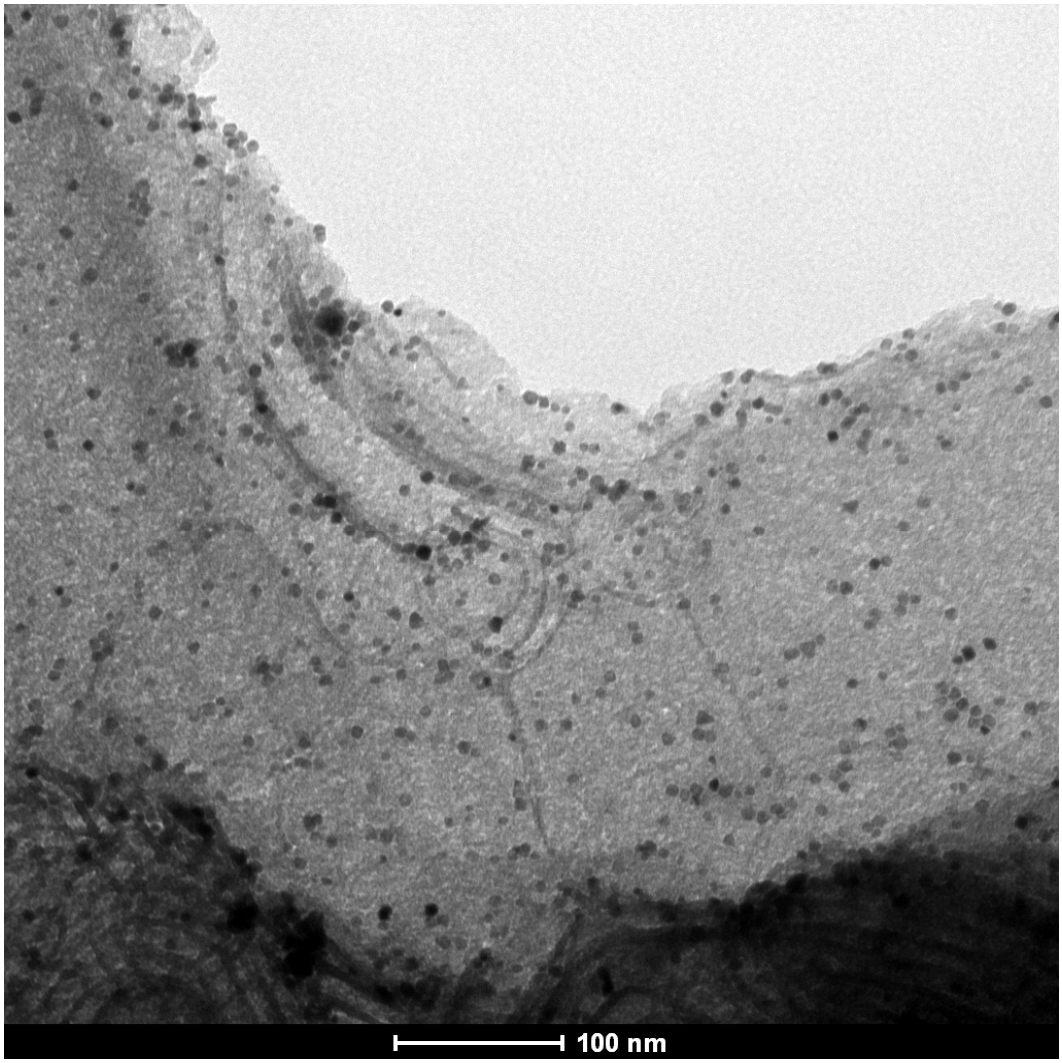

Figure S12. TEM image of Au-Rh core-shell NPs with a thick Rh layer supported on amorphous silica.

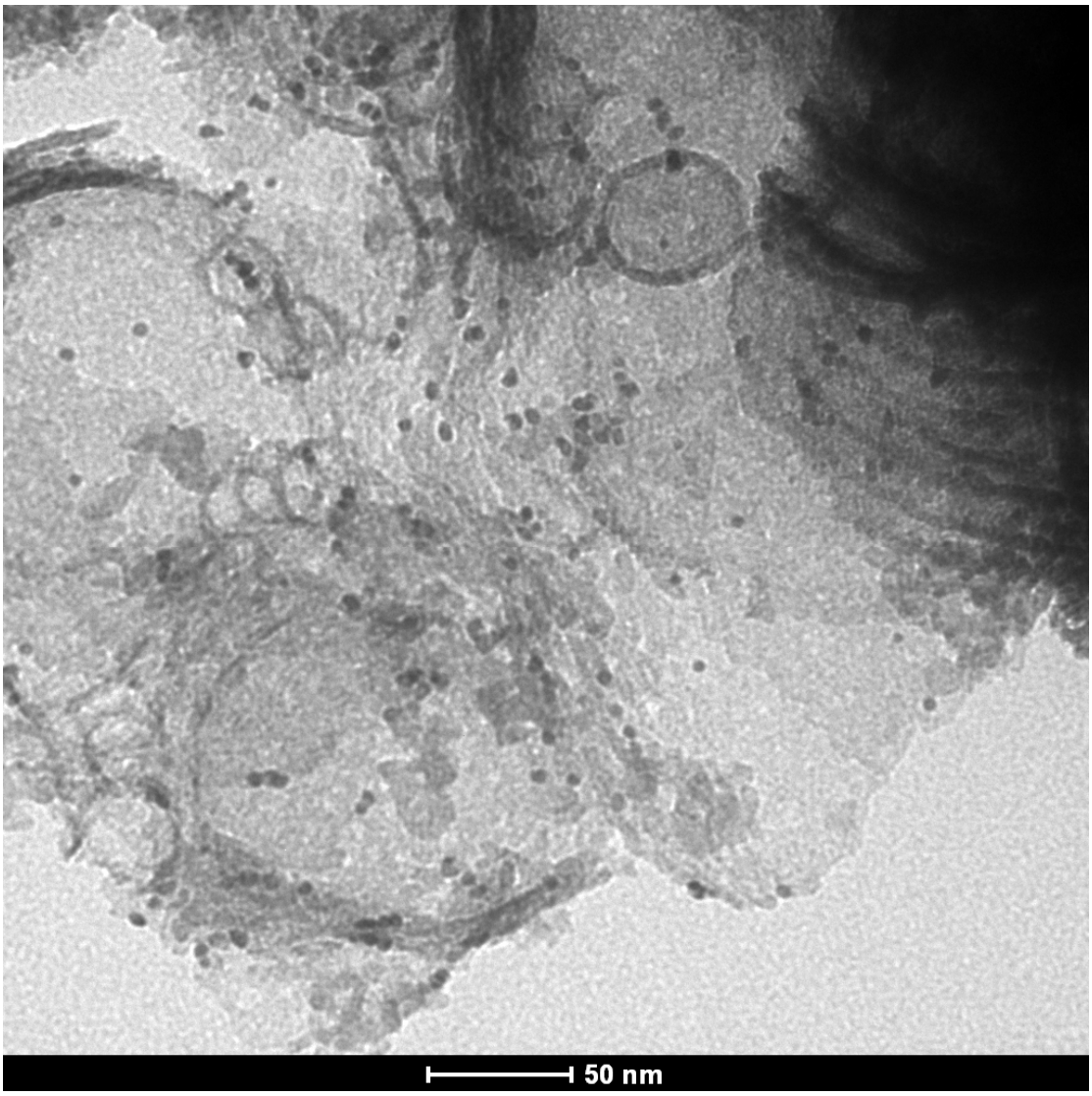

Figure S13. TEM image for Au-Rh core-shell NPs with an average of 2.5 Rh monolayers supported on amorphous silica, after catalytic studies were performed.

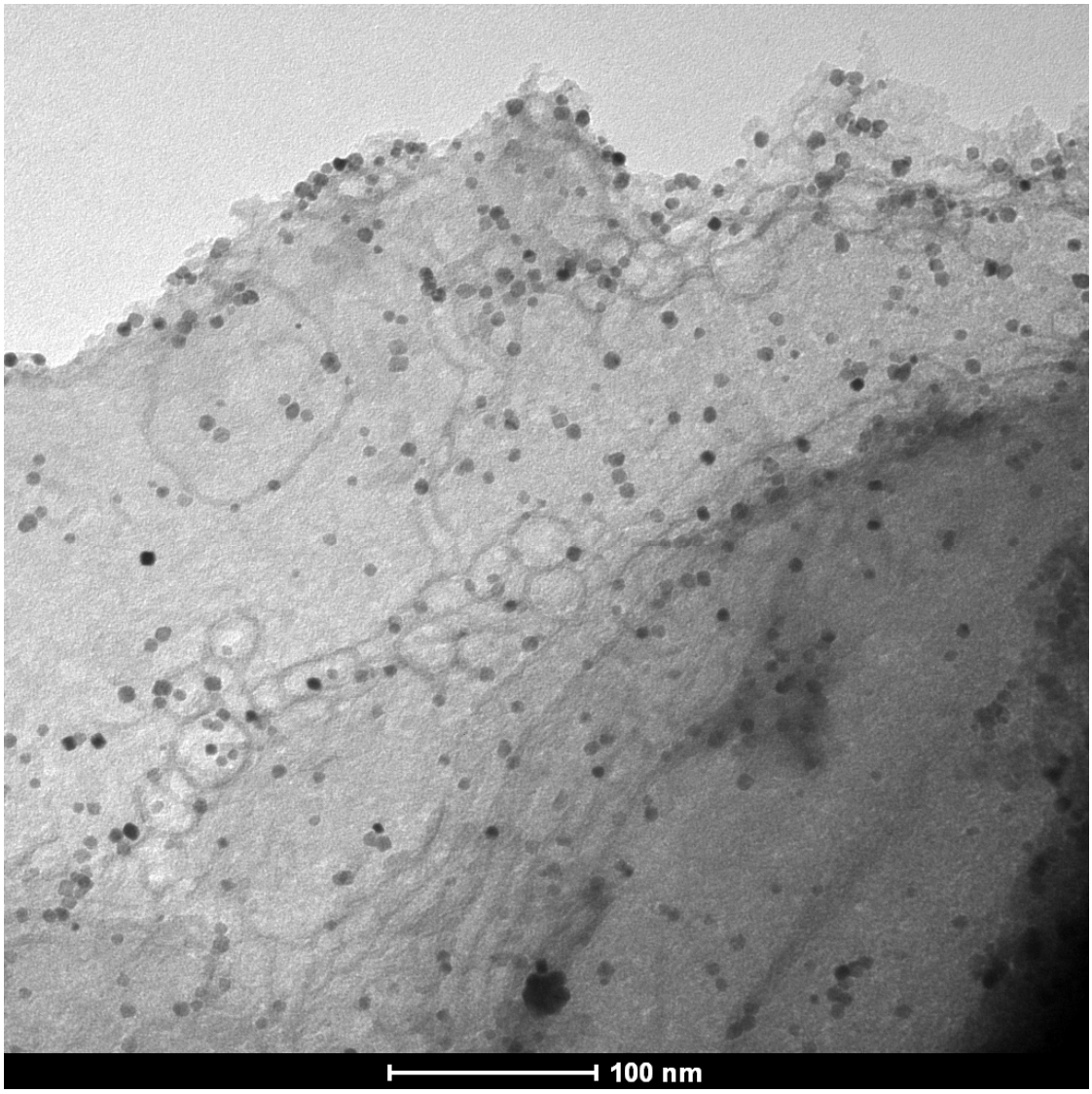

Figure S14. TEM image for Au-Rh core-shell catalyst with a thick Rh layer after catalysis was performed.

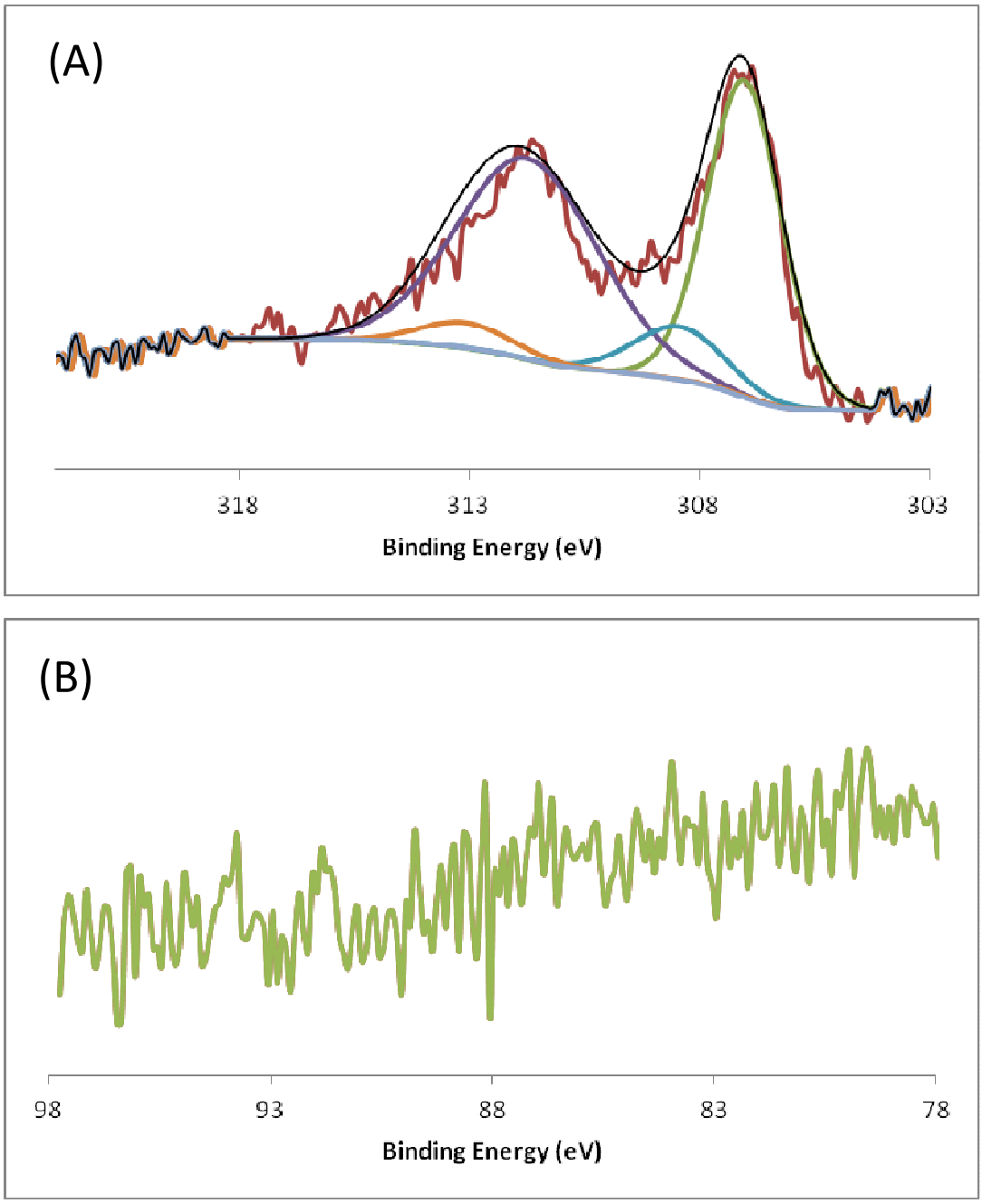

Figure S15. Fitted XPS data for Au-Rh core-shell NPs with a thin Rh layer supported on amorphous silica post- catalytic studies; (A) Rh 3d signals assigned to Rh(0) (307.0 eV) and Rh(I) (308.4 eV); (B) Absence of Au 4f signals confirming that no Au is present on the surface.

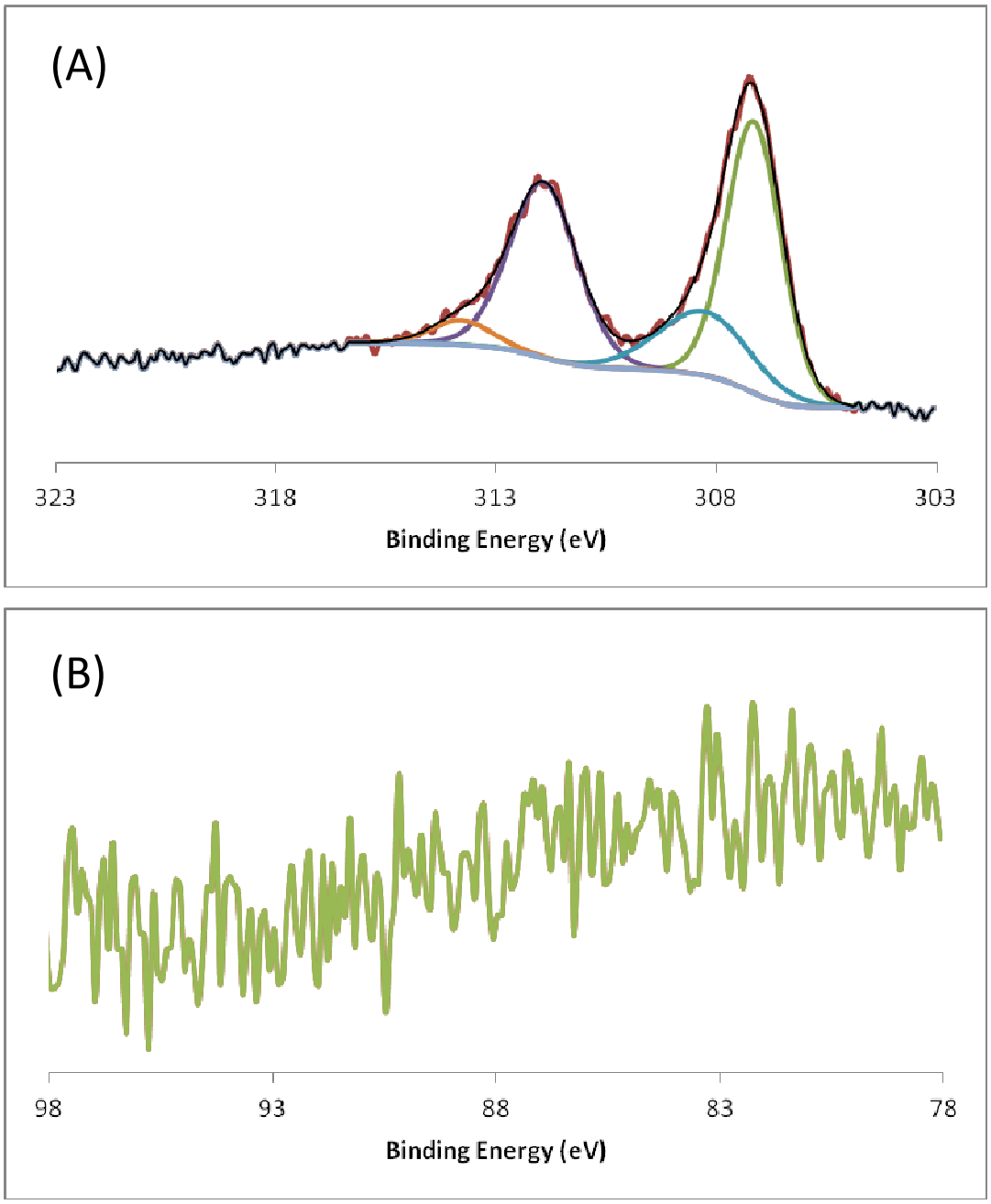

Figure S16. Fitted XPS data for Au-Rh core-shell NPs with an average of 4 Rh monolayers supported on amorphous silica, after catalytic studies were performed; (A) Rh 3d signals corresponding to Rh(0) (307.1 eV) and Rh(I) (308.3 eV); (B) Absence of Au 4f signal.

Table S4. Rh(I):Rh(0) and Au(X):Rh(X) ratios, based on XPS values, for thin-Rh and thick-Rh core-shell catalysts after catalytic studies were performed.

	Rh(I) : Rh(0)	**Au : Rh**
Thin-Rh NPs	1 : 5	0 : 1
Thick-Rh NPs	1 : 2.5	0 : 1

Experimental Section

Materials. Rhodium trichloride hydrate ($RhCl_3 \cdot xH_2O$, 98%; Johnson Matthey), hydrogen tetrachloroaurate ($HAuCl_4.3H_2O$, 98%; Sigma Aldrich), sodium borohydride ($NaBH_4$, 98% ; Sigma Aldrich), poly(vinylpyrrolidone) (PVP, $<M_w>$ = 55,000; Sigma Aldrich), ethylene glycol ($\{CH_2OH\}_2$, 99.8%; Fisher Scientific) and 1-cyclohexene (C_6H_{10}, 99%; Alfa Aesar) were used as received. All other reagents and solvents (analytical grade) were employed without further purification unless stated otherwise. TEM grids (200 mesh Cu/Formvar; Ted Pella, Inc.) were prepared by drop-casting ethanol solutions of Au and Au/Rh NPs that were evaporated to dryness in air. Samples for TOF SIMS and XPS analysis were prepared by drop-casting ethanol solutions of the particles on ITO coated glass wafers allowing evaporation of the solvent in air.

Methods. A MARS 5 (CEM Corp.) microwave system with a maximum power of 1600 W (2.45 GHz) was used to perform all the NP synthesis reactions. The reaction temperature inside the microwave cavity was finely controlled by power modulation *via* a RTP-300+ fiber optic temperature, located in a beaker of solvent identical to that employed in the reaction. *Note: Insertion of the temperature probe directly into the reaction vessel should be avoided; build-up of solid RhNP product on the probe sheath during the course of the reaction may lead to sparking and ignition.* A 25 mL round-bottom flask with a side-arm inlet and fitted with a water-cooled reflux condenser was placed in the center of the microwave chamber. Both solvent and reactants were magnetically stirred (medium speed setting) and the Rh precursor was then added into the solvent using a disposable, fine-bore Teflon tube right above the solution, ensuring that the addition rate was constant. The rate of Rh precursor addition was controlled using an Aladdin Programmable Syringe Pump (WPI, Inc.) that was directly attached to the Teflon tubing. The reactions were carried-out at ambient pressure in air, with venting at the top of the reflux condenser *via* a three-way stopcock. Prior to each new reaction, glassware was thoroughly cleaned in a two-stage acid-base wash (12.0 M HCl aq., 1−2 d; 5 M NaOH in *i*-PrOH/H2O, 1−2 d), followed by oven drying at 110 °C.

Characterization. Transmission Electron Microscopy (TEM) images were obtained from a FEI Tecnai microscope operating at 80 kV. The samples were prepared by drop-casting a single aliquot of nanoparticles dispersed in ethanol onto 200 mesh carbon coated copper formvar grids (Ted Pella Inc.) and allowing for subsequent evaporation in air. Nanoparticle sizes and standard deviations were derived by measuring a minimum of 200 individual particles per experiment, and by averaging multiple images from samples obtained from at least two separate syntheses. Individual particles were measured using Image-J (http://rsbweb.nih.gov/ij), which finds the area of each nanoparticle by pixel counting. High-resolution TEM (HRTEM) and energy dispersive X-ray analysis (EDX) were performed using a JEOL 2010F transmission electron microscope. This instrument was operated at 200 keV using a field-emission gun with 0.19 nm point-to-point resolution. Powder X-ray diffraction patterns were recorded with a Bruker AXS D8 diffractometer using a Cu Ka source (1.5418 Å) operated at 40 kV and 40 mA; spectra were collected using a scan speed of 3° min^{-1} with a step width of 0.020 (2θ). UV-vis data were collected using a Carry 6000i UV-vis NIR spectrometer equipped with a double beam and a wavelength range of 175−3300 nm. Time-of-Flight Secondary Ion Mass Spectrometry (TOF SIMS) analysis were done using a

TOF.SIMS 5 instrument (ION-TOF GmbH, Germany 2010), which used a primary ion beam (Bi_1^+, 30 keV, 2.8 pA measured sample current) to raster-scan an area of 200 x 200 μm^2. The actual sputtering was done using a Cs^+ ion beam (500 eV energy, 63 nA measured sample current) on a 500 X 500 μm^2 area centered on the probing area. Due to strong charging of the surface, a constant, low energy electron beam (21 eV) was directed on the samples at all times during data acquisition for charge compensation. All detected secondary ions had negative polarity. X-ray photoelectron spectroscopy (XPS) was performed using a Kratos Axis Ultra Photoelectron Spectrometer. The XPS spectra were recorded utilizing a monochromated Al-K_a x-ray source (hγ=1486.5 eV), hybrid optics (employing a magnetic and electrostatic lens simultaneously) and a multi-channel plate coupled to a hemispherical photoelectron kinetic analyzer. All spectra were recorded using four sweeps for signal averaging, a dwell time of 1800 msec, an aperture slot of 300 x 700 µm, a pass energy of 20 eV and 0.1 eV per step. To minimize sample charging and band shape distortion due to charging, the XPS spectra were recorded using the Kratos charge neutralizer (20 eV electrons) while the sample stage was left floating (i.e. not connected to ground (earth)). The effectiveness of the neutralizer under these conditions notably improved the resolution of the spectra since, for example, the Au 4f bands of the reference PVP-capped MwH-AuNPs were significantly sharper with a small tail in the high binding energy side of this transition. This tail may also be a contribution from oxidized Au atoms. Casa XPS analysis software was used for peak deconvolution and the stoichiometry of samples was determined from corrected peak areas and employing Kratos sensitivity factors for each element of interest. X-ray absorption spectroscopy (XAS) data were collected at beamline X18B at the National Synchrotron Light Source at Brookhaven National Laboratory. Between 115-130 mg of the SiO_2 supported NPs were pressed at a pressure of 3 tons for 30 s to form a pellet for analysis. Reference foils were collected in transmission mode between I_o and I_t gas ionization chambers and the data fit to yield the amplitude reduction factors for each edge. For the Au L_3 edge spectra, I_0 was purged with N_2 and I_t purged with 50% Ar and 50% N_2. For the Rh K edge spectra, I_0 was purged with Ar and I_t with 80% Ar and 20% Kr. For the pellet analysis I_0 was the same as for the respective foils, but the spectra were collected in fluorescence mode using a passivated implanted planar silicon (PIPS) detector. The data were analyzed using the IFFEFIT software package.[a] Simultaneous first shell fitting of both edges was done using a k-weight of 2 and by constraining the bond length and Debye-Waller factors for the Au-Rh and Rh-Au scattering paths to be equivalent.

Synthesis of Au seeds. A solution of poly(vinylpyrrolidone) (200 mg, 1.8 mmol) and sodium borohydride (20 mg , 0.52 mmol) in ethylene glycol (15.0 mL) was prepared directly in the reaction vessel and brought to 150 ℃ with stirring. A second solution of $HAuCl_4.3H_2O$ (20 mg, 0.05 mmol) was prepared in the same solvent (5.0 mL) and loaded into a fresh 10 mL disposable syringe. For the preparation of Au seeds, 5 mL of the precursor solution was injected into the hot stirred PVP solution at a rate of 3 mmol h^{-1} (300 mL h^{-1}). The color of the solution became rapidly red /pink. The mixture was stirred for an

[a] http://cars9.uchicago.edu/~newville/Papers/JSR_PH5149.pdf. Newville, M. J. Synchrotron Radiat. 2001, 8, 322−324.

additional 30 minutes at 150 ℃ after completion of the precursor addition. The reaction was then cooled rapidly by transferring the reaction vessel to an ice-water bath. The Au NPs seeds were precipitated by adding acetone (*ca.* 60 mL) to give a red brown suspension, which was briefly sonicated (1 min). The precipitate was then isolated by ultracentrifugation (5 krpm, 5 min) and the colorless supernatant was decanted away to leave a red brown solid. This was further purified to remove excess PVP and ethylene glycol by 3 cycles of dissolution in ethanol (15 mL) followed by precipitation with hexane (75 mL) and isolation by centrifugation.

Controlled growth of Rh over Au cores. A suspension of Au seeds was prepared directly in the reaction vessel by dissolving 3 mg of dried Au NPs and poly(vinyl pyrrolidone) (200 mg, 1.8 mmol) in ethylene glycol (15 mL), and it was then brought to 150 ℃ with stirring. A second solution of $RhCl_3 \cdot xH_2O$ (10 – 40 mg, 0.048 – 0.19 mmol) was prepared in the same solvent (5 mL) and loaded into a fresh 10 mL disposable syringe. The Rh solution was added into the hot stirred PVP/Au suspension at a rate of 20 mL h^{-1}. The Rh shell thickness was controlled by the concentration of the Rh solution, which affected the addition rate in terms of mmol of metal added per unit of time (0.19 mmol h^{-1} – 0.76 mmol h^{-1}). The red color of the initial Au suspension rapidly became brown after the injection of the Rh precursor. The mixture was then stirred for an additional 30 minutes at 150 ℃ after the Rh precursor was added. After this period, the reaction was cooled down using an ice-water bath and the resulting particles were extracted and purified as stated above for the Au seeds.

Catalytic Studies. The catalysts were prepared by addition of pre-calcined SiO_2 (200 mg) to suspensions of 5-7 mg of PVP-capped Au and Au/Rh NPs in ethanol/H_2O (1:1). The slurries were sonicated for 20 min, isolated by filtration, washed with ethanol/H_2O and dried at 65 ℃. For each catalytic study, a small amount of the composite catalyst (*ca.* 5 – 30 mg) was loaded into a custom made quartz U-tube, suspended above a D3-porosity frit. The sample was mixed in with acid washed and calcined sand, heated to 25 ℃ and then the sample and entire reactor line (quartz, heated to 90 ℃) was purged with the reactant gas mixture (H_2/He 1:1) for 30 min. Catalysis began with the introduction of cyclohexene vapor into the gas stream *via* an in-line saturator fitted with fritted bubbler. All data was obtained in – real-time by automated pneumatically-gated sampling of the exhaust stream, directly into an HP Agilent 6890 GC fitted with Restex Stabiliwax 15 m column and tendem FID and TCD detectors. Activity and turnover frequency values were obtained based on estimated surface area-to-volume ratios (by TEM). The activity was calculated by multiplying the product of the rate of injection of the reactant and the normalized area of cyclohexane by the grams of catalyst. The area of the cyclohexane peak (GC data) was normalized by dividing the area count by the molecular weight of the compound (Eq. 1). This value was then divided by the sum of the normalized values for both product and reactant (cyclohexane and cyclohexene).

$$\text{g catalyst} \times \left[\frac{\mu\text{mol Cyclohexene}}{\text{min}} \times \frac{\dfrac{\text{Area count}_{\text{Cyclohexane}}}{MW_{\text{Cyclohexane}}}}{\dfrac{\text{Area count}_{\text{Cyclohexane}}}{MW_{\text{Cyclohexane}}} \times \dfrac{\text{Area count}_{\text{Cyclohexene}}}{MW_{\text{Cyclohexene}}}} \right] \qquad \textbf{Eq. 1}$$

The turnover frequency values were calculated by dividing the activity (in mol g^{-1} s^{-1}) by the product of the normalized Rh loading value and the number of bulk atoms to surface atoms ratio (PME value) (Eq. 2). To account for the fact that the particles are not entirely composed of Rh atoms, the previous value was multiplied by the inverse of the average % of Rh atoms in each NP. The normalized percent Rh loading was acquired by dividing the value for wt% Rh in the catalyst by the atomic weight of Rh. High resolution ICP-MS data was used to determine the total mass %Rh and %Au loading.

$$\frac{1}{\text{Avg. \% Rh atoms on NP}} \left[\frac{\text{Activity Cyclohexane (mol g}^{-1}\text{ s}^{-1}\text{)}}{\frac{\text{Wt \% Rh in catalyst}}{AW_{Rh}} \times \text{PME}} \right] \qquad \textbf{Eq. 2}$$